Energy Conversion and Management: X 26 (2025) 100957

Contents lists available at ScienceDirect

Energy Conversion and Management: X

journal homepage: www.sciencedirect.com/journal/energy-conversion-and-management-x

A mathematical model for hybrid-electric propulsion system for regional propeller-driven aircraft

Giuseppe Grazioso *, Mario Di Stasio, Fabrizio Nicolosi, Salvatore Trepiccione

University of Naples Federico II, Department of Industrial Engineering, Via Claudio, 21, Naples, 80125, NA, Italy

ARTICLE INFO

Keywords:
Aeronautics
Hybrid-electric powerplant
Powerplant modeling
Power management

ABSTRACT

To address the environmental challenges in aviation, this research presents a novel mathematical model for simulating hybrid-electric powerplants in regional propeller-driven aircraft from the early design stages. The model integrates conventional thermal engines with battery and fuel cell systems, supporting up to two independent propulsion lines. Using a throttle-based approach, a linear mathematical formulation estimates power distribution within the architecture. A powerplant management algorithm enhances adaptability to varying power demands while ensuring a physically consistent solution. This approach enables rapid performance evaluation, allowing designers to optimize configurations from the earliest design stages. Case studies validate the model's effectiveness in meeting diverse power requirements while maintaining a consistent solution. Ultimately, this study provides innovative analytical method for early-stage exploration and optimization of complex propulsion systems, contributing to a more sustainable aviation sector.

1. Introduction

Aviation accounts for about 3.8% of Europe's greenhouse gas (GHG) emissions, with projected annual growth of roughly 4.5% [1,2], highlighting the need for innovative decarbonization strategies. In response, the European Union (EU) has outlined in its *Fly The Green Deal* roadmap [3] ambitious emissions reduction targets for 2030, 2035, and 2050 towards net-zero CO_2 emissions. Hybrid-electric (HE) and all-electric (AE) propulsion systems represent a promising pathway toward more sustainable aviation, as they can significantly reduce or even eliminate direct and indirect CO_2 emissions [4,5]. These strategies combine thermal engines with alternative energy sources such as batteries or fuel cells.

Within this broader context, regional propeller-driven aircraft offer a particularly attractive testbed for hybridization considering their lower power demand if compared with larger aircraft. Moreover, short-haul flights under 600 nautical miles represent approximately 55% of global flight operations and are responsible for about 18% of the sector's CO_2 emissions [6]. Regional aircraft can operate from shorter runways and access a wider airport network, improving connectivity in areas with limited infrastructure. Additionally, forecasts by ATR and Bombardier predict strong growth in this market segment, driven by fleet replacements and increasing passenger demand [7,8].

HE propulsion systems that couple thermal engines with battery-powered electric motors are attracting increasing interest. The feasibility and environmental benefits of such systems are strongly influenced by battery energy density and weight constraints, making them particularly suitable for regional aircraft applications. Pornet and Isikveren [9] investigated a narrow-body transport aircraft equipped with two advanced geared turbofan engines and two under-wing podded electrical fans powered by batteries, demonstrating that a 16% reduction in fuel burn could be achieved for short-range missions with an 18% battery energy ratio. Voskuijl et al. [10] analyzed a 70-passenger regional turboprop aircraft where Li-air batteries supplied 34% of the shaft power, resulting in a 28% emission reduction for a 825 nm range mission. Similarly, Marciello et al. [11] conducted a design exploration for a 50-passenger regional aircraft using internal combustion engines paired with batteries. They projected fuel savings of 24% in the short-term (2025–2035), which rise up to 45% in the medium-term (2035–2045) with improvements in battery energy density. Nasoulis et al. [12] provided an in-depth environmental and techno-economic assessment of HE propulsion architectures with thermal engines and batteries, showing that, for a 19-seat commuter aircraft, series configurations could reduce environmental impact by up to 59.7% compared to conventional aircraft by 2040, albeit with higher capital costs than parallel configurations. These studies indicate that an increase in the hybridization ratio does not necessarily correspond to a reduction in fuel consumption. Instead, fuel savings reach a minimum point before beginning to rise again. This nonlinear trend is also supported by Viswanathan et al. [13], who demonstrate that the low gravimetric energy density

* Corresponding author.
E-mail address: giuseppe.grazioso@unina.it (G. Grazioso).

https://doi.org/10.1016/j.ecmx.2025.100957
Received 3 January 2025; Received in revised form 28 February 2025; Accepted 5 March 2025
Available online 14 March 2025

of current Li-ion batteries (approximately 280 Wh/kg [14]) represents the actual bottleneck in achieving greater fuel reduction. However, as demonstrated by Reid et al. [15], optimizing power management throughout the design range during the design loop can mitigate the limitations imposed by low battery energy density. Current studies on AE propulsion systems based on batteries are generally restricted to small general aviation aircraft, primarily due to the gravimetric energy density limitations discussed above. Hospodka et al. [16] provided valuable insights into the trade-offs between battery mass and operational performance for small commuter aircraft, highlighting that AE aircraft can deliver substantial operational cost advantages despite these constraints.

Greater fuel reduction is potentially achievable by substituting the battery system with a higher energy density power source, such as a fuel cell system [17]. Palladino et al. [18] conducted a conceptual design analysis of a 70–80 seat regional aircraft utilizing HE propulsion powered by hydrogen fuel cells. Performance assessments were conducted for various configurations of the electrical propulsion system and different mission profiles. The findings revealed that, compared to a conventional baseline aircraft, the optimal hybrid configuration achieved a 24% reduction in CO_2 equivalent emissions and a 40% decrease in NO_x emissions, highlighting the potential of fuel cell technology to significantly mitigate the environmental impact of regional air travel. Similarly, Rischmüller et al. [19] explored the retrofit of the Dornier 328 regional aircraft to incorporate a hydrogen-hybrid dual-fuel propulsion system. The findings revealed that, compared to the original aircraft, the optimal hybrid configuration achieved an 18% reduction in fuel consumption. Recent studies have expanded the scope of hybrid-electric architectures by integrating multiple power sources to enhance performance and endurance. Ji et al. [20] proposed a novel hybrid propulsion and power system combining batteries, fuel cells, and jet engines for a high-altitude, long-endurance unmanned aerial vehicle configuration. The examined aircraft, with specifications similar to the Northrop Grumman RQ-4 Global Hawk, featured a maximum operating altitude of 27.5 km, with a top Mach number of 1.8. The hybrid configuration was designed so that batteries provided high thrust during take-off, while solid oxide fuel cells powered the electric motors during cruise, supplying continuous electrical power with minimal fuel consumption. The results indicated that this hybrid system could achieve an endurance of 19.6 h during cruise operations, with a thrust-specific fuel consumption of 15.32 g/s/kN. Importantly, the integration of fuel cells contributed to a significant reduction in fuel consumption during the cruise phase without imposing substantial weight penalties. The findings highlight the potential of combining fuel cells and batteries to meet the power and energy requirements across all flight segments.

Fully electric configurations may offer even larger environmental benefits, particularly when fuel cells are integrated with high-energy-density battery systems. In their 2023 study, Eissele et al. [21] designed a 50-passenger regional aircraft intended for entry into service by 2040, combining both hydrogen fuel cells and batteries for propulsion. Innovative features, such as wingtip propellers, were integrated too, to enhance performance and sustainability even further. The study concluded that, while fuel cell-based AE regional aircraft are promising and feasible by 2040, further research is needed in fuel cell technology and thermal management, to fully realize their potential. In their 2023 study, Sparano et al. [22] developed a mathematical tool to co-design a hybrid powertrain for regional aircraft, integrating hydrogen fuel cells and batteries. Their findings suggest that such hybrid systems are feasible and highlight the potential of hydrogen fuel cells in achieving more sustainable aviation.

In contrast to these hybrid approaches, several studies demonstrate the feasibility of a fully electric powerplant employing a purely hydrogen fuel cell system. For instance, Zaghari et al. [23] illustrate the scalability of a multi-stack fuel cell system for regional aircraft. The authors explored various configurations in which fuel cell stacks are connected in parallel and series to meet power demands, assessing their impact on system efficiency, total weight, failure management, and operational performance. Key findings indicate that configurations providing independent control over fuel cell stacks through individual DC/DC converters offer better fault tolerance and operational flexibility but at the cost of increased weight and reduced overall efficiency. Additionally, the study highlights critical trade-offs between system voltage levels, power converter design, and weight penalties. To support and improve the design of fuel cell systems tailored for AE aircraft applications, Li et al. [24] developed a graphical design approach based on mission-specific requirements. They demonstrated that with their approach, the cruise powertrain specific energy can be improved by 6.5%.

While the above literature clearly indicates that HE powerplants incorporating hydrogen-based fuel cell systems can significantly reduce aviation emissions, there are several issues and shortcomings which need to be addressed as well. Schenke et al. [25] and Hoelzen et al. [26] have highlighted that a robust hydrogen supply chain is essential for the effective integration of hydrogen in aviation. Moreover, Hoelzen et al. [27] emphasize the importance of developing a strategic hydrogen refueling system aligned with the hydrogen supply chain. In addition to electrification strategies, alternative fuels like sustainable aviation fuel (SAF) have emerged as a viable means to decarbonize aviation without extensive modifications to existing infrastructure. Alrebei et al. [28] evaluated a novel SAF derived from multiple biomass feedstocks, demonstrating its compatibility with the CFM56-7B turbofan engine without requiring design alterations. Notably, the proposed SAF outperformed conventional Jet A1 fuel, achieving a 17% thrust increase and a 10% range improvement, while also reducing CO_2 emissions by up to 8%. These findings underline the potential of SAF as a transitional solution in hybrid propulsion configurations, where thermal engines can operate more efficiently alongside electric power sources.

To accurately assess the benefits of integrating thermal engines, batteries, and fuel cells in HE or AE configurations, robust and straightforward analysis methods are needed, especially in the early design phases when time and data are limited. The literature offers several strategies to simplify the modeling of two-sources hybrid powerplants. Early work by Nam et al. [29] estimated output power based on two distinct power paths, using fixed component efficiencies and a power fraction concept. Buecherls et al. [30] introduced the hybridization factor described by Eq. (1), where P_1 and P_2 are respectively the primary and secondary source produced power. This parameter has been later combined by Pornet et al. [31,32] with power path models to represent parallel HE architectures.

$$\phi = \frac{P_2}{P_1 + P_2} \tag{1}$$

De Vries et al. [33] proposed a generalized two-source HE architecture integrating two propulsive lines. This architecture can be specialized to nine distinct power paths, referred to as *operation modes*. To interact with this architecture, they introduced the *supplied power ratio*, defined as in Eq. (1), where $P_2 = P_{BAT}$ represents the power generated by the battery, and $P_1 = P_{fuel}$ denotes the power produced by fuel combustion. In addition, they defined the *shaft power ratio* Φ (Eq. (2)), which quantifies the fraction of secondary shaft power P_{S_2} relative to the total produced shaft power, and the *thrust power ratio* χ (Eq. (3)), which specifies the fraction of thrust generated by the secondary propulsive line relative to the total thrust. Assuming steady-state conditions and constant component efficiencies, the power distribution within the propulsion architecture can be determined, for a given combination of required propulsive power (P_P), Φ, and ϕ, by selecting a specific *operation mode* and solving a set of *powertrain equations*, which form a linear system of ten equations with ten unknowns.

$$\Phi = \frac{P_{S_2}}{P_{S_1} + P_{S_2}} \tag{2}$$

$$\chi = \frac{T_2}{T_1 + T_2} \tag{3}$$

By contrast, Palaia et al. [34] presented a direct method that models a two-source hybrid-electric powerplant without relying on powertrain equations. The proposed approach features a two-source parallel configuration in which a thermal engine and a battery pack work together to supply a single propulsive line through an electric machine and a gearbox. Their approach begins by assigning a fixed power fraction to the thermal engine. Subsequently, based on the estimated propulsive power demand necessary to meet the aircraft's mission flight requirement, it is possible to determine the power that must be delivered by the battery and the thermal engine. Although this formulation offers a straightforward and explicit approach, its applicability is limited to parallel architectures only, and does not consider the possibility of battery recharging during flight.

Alternative approaches to model HE powerplants rely on high-fidelity simulation models, that can be produced by using behavioral modeling tools like MATLAB/Simulink[1] or Amesim.[2] With these tools, the designer can accurately model complex powerplant systems capturing the component transient dynamics and the non linear interactions among the architecture. For instance, in relation to fuel cell systems, Schröder et al. [35] developed a computationally efficient one-dimensional, two-phase polymer electrolyte membrane fuel cell stack model for commercial aircraft applications, emphasizing the importance of water management and optimized stack operating conditions. Extending this work, Schröder et al. [36] proposed a comprehensive fuel cell-based propulsion system for a 70-passenger regional aircraft, incorporating Pareto optimization to balance mass, drag, efficiency, and volume. However, interacting with these high-fidelity simulation models requires designing, tuning, and testing a dedicated power management controller, a demanding process that is often impractical in early-stage analysis. Power controllers can be developed using three main strategies: (i) rule-based energy management [37], (ii) optimization-based methods [38,39], (iii) learning-based approaches [40]. A comprehensive discussion on high-fidelity simulation methods is available in [41,42].

Between the two above-mentioned powerplant modeling concepts, a mid-fidelity approach offers a balanced alternative. With this kind of approach, each powerplant component is represented by a specific mathematical formulation that captures its behavior using a reduced number of variables. Power output and distribution are estimated by solving an optimization problem. When these formulations are integrated with the power requirements derived from a specific mission trajectory, the optimal power management strategy for a given flight profile can be determined. Different techniques can be used to solve this optimization problem. For example, Leite et al. [43] address the optimal energy management problem for a two-source HE powerplant using dynamic programming. Doff-Sotta et al. [44,45] reformulate the same optimization problem as a convex optimization task improving the convergence rate, while Li et al. [46] apply a fuzzy-logic controller to optimize the energy distribution in a fully electric, two-source powertrain architecture.

Current modeling strategies lack simple methods for analyzing powerplants integrating three energy sources over two propulsive lines. High-fidelity methods are too complex and time-consuming to be used to analyze the powerplant behavior during the preliminary design, due to limited available data. As a result, designers often rely on the methods by Palaia [34] and De Vries [33], which are limited to two energy sources and need to be adapted for a third source. Palaia's approach provides an explicit formulation for modeling HE architectures; however, its applicability is limited only to parallel architectures. In contrast, De Vries' approach allows designers to model more general architectures. Although it is based on the definition of *supplied power ratios*, which are particularly suitable during the preliminary sizing of powerplants for aircraft applications, its effectiveness diminishes when designers need to evaluate the performance of a preliminarily sized architecture. In such cases, greater control over each energy source's contribution is essential to better understand how each of them influences the overall powerplant performance. Additionally, when inappropriate choices are made regarding the *operation mode*, Φ, ϕ, and P_P the method can result in negative power outputs, indicating an unbalanced energy distribution among the architecture. Therefore, to address these inconsistencies, designers must either adjust the hybridization factor or select an alternative *operation mode* to achieve a consistent solution.

To address these limitations, this article proposes a hybrid-electric powerplant model integrating thermal engines, fuel cells, and batteries, controlling their contribution by selecting their throttle settings. Here, the throttle setting is defined as the ratio of the actual output power delivered by an energy source to its maximum deliverable output power. This approach yields a linear, explicit mathematical representation of the power distribution among the architecture without relying on large equation systems. Moreover, to always ensure consistent solutions, the authors have introduced a powerplant management algorithm based on simple rules rather than complex control logic. If necessary, it can alter the *operation mode* or throttle settings to meet the required propulsive power while adhering closely to designer-defined parameters. Therefore, the proposed powerplant model supports the designer in analyzing, from the early design stages, the performance of HE architectures integrating up to three different power sources and two separate propulsive lines, while guaranteeing a reliable outcome at all times.

The content of this paper is organized as follows. Section 2 presents a simplified method for modeling the behavior of a three-source hybrid-electric powerplant system for propeller-driven aircraft. In particular, Section 2.1 provides details about the models used to represent each sub-component of the powerplant and presents two different control strategies employed to simulate the powerplant's behavior depending on whether a specific propulsive power requirement must be satisfied. Section 2.2 describes a dedicated powerplant management algorithm developed to assist designers, ensuring that specific power requirements are met while maintaining a physically consistent behavior. Section 3.1 demonstrates the applicability of the proposed powerplant model by showing how the powerplant system satisfies different power requests based on the selected operational settings. Subsequently, Section 3.2 demonstrates the applicability of the proposed powerplant model to the analysis of the cruise phase of a preliminarily sized three-source HE regional propeller-driven aircraft, designed to transport 90 passengers over 600 nmi. Finally, Section 4 presents the conclusions and outlines future work.

2. Materials and methods

2.1. Hybrid-electric powerplant model

System architecture, operating modes, and modeling principles

Simulating the behavior of an HE powerplant during the preliminary design phase requires adopting a simple and flexible approach. The proposed method supports designers in evaluating the ability of a preliminarily sized powerplant to meet specific performance or mission objectives, ensuring reliable power distribution and avoiding physical inconsistencies. To achieve this, the study presents a simple mathematical formulation to simulate a generalized three/source powerplant architecture and a dedicated power management algorithm to preserve a consistent power distribution.

The proposed model enhances the conventional two-source approach, widely discussed in the literature, allowing for the analysis of more complex configurations. Three energy sources are integrated: a gas turbine (GT), a fuel cell (FC), and an electric storage system

[1] https://it.mathworks.com/products/matlab.html

[2] https://plm.sw.siemens.com/it-IT/simcenter/systems-simulation/amesim/

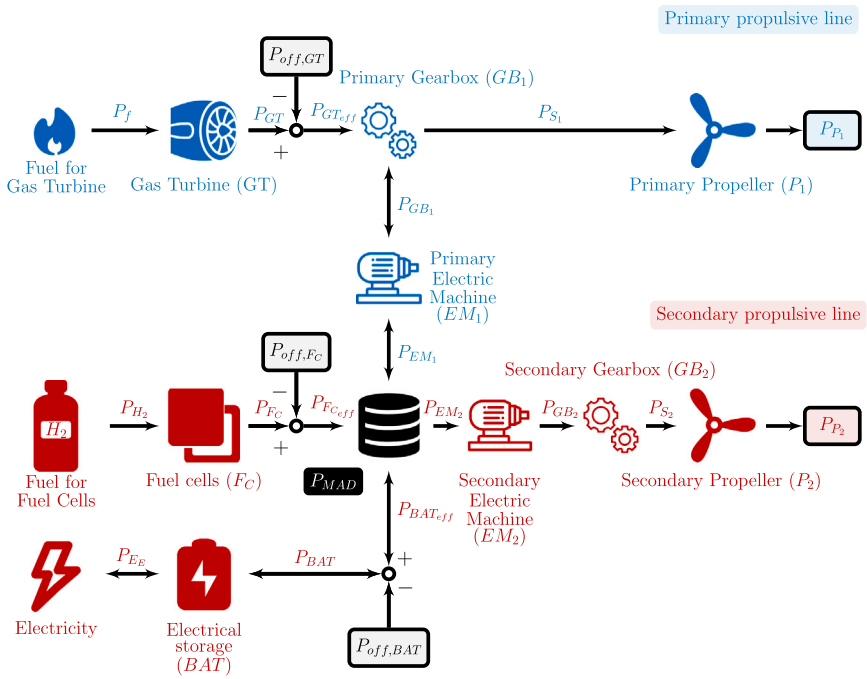

Fig. 1. Hybrid-electric powerplant architecture integrating three different power sources — thermal engines, fuel cell systems and battery — and two distinct propulsive lines.

Table 1
Operating modes of the hybrid-electric powerplant architecture, defined by the roles of the primary electric machine (EM_1) and the electric storage system (BAT). When EM_1 operates as a motor, electrical energy is converted into mechanical energy, transferring power from the $PMAD$ node to GB_1. Conversely, when EM_1 operates as a generator, mechanical energy is converted into electrical energy, transferring power from GB_1 to the $PMAD$ node.

Operation mode	Primary electric machine	Electric storage
1	Motor	Discharge
2	Motor	Charge
3	Generator	Discharge
4	Generator	Charge

(BAT), which collectively drive two independent propulsion lines. A power management and distribution ($PMAD$) unit works as a power hub, providing the required shaft power distribution and allocating the necessary power through the electric machines (EM_1, EM_2) and gearboxes (GB_1, GB_2). Fig. 1 illustrates the proposed HE architecture and highlights the power flows among its components. P_F denotes the power derived from combusted fuel, while P_{GT} represents the power output from the gas turbine. The power extracted from hydrogen is indicated by P_{H_2}, and P_{FC} refers to the power produced by the fuel cell system. P_{BAT} denotes the power either delivered to or drawn from the electric storage system. Each energy source can also feature a specific power extraction ($P_{off_{source}}$), which reduces its output to an effective usable power, $P_{source_{eff}}$. The mechanical power on the propulsion shafts is expressed as P_{S_1} and P_{S_2}, while the propulsive power generated by the propellers is denoted by P_{P_1} and P_{P_2}.

A key aspect of this three-source architecture is its operational flexibility, obtained by switching the role of the primary electric machine (EM_1) between motor and generator modes, along with the charge or discharge behavior of the battery. This aspect allows the proposed architecture to specialize in four distinct *operation modes*, enabling designers to tailor power flows to specific mission requirements. These four distinguished behaviors are summarized in Table 1. Caution is required to avoid physically inconsistent scenarios. For example, in *mode 2* the battery is charging and EM_1 acts as a motor. If the battery's requested charge power exceeds the fuel cell output power, contradictory demands may arise at the PMAD node. The power management algorithm (described in Section 2.2) addresses such inconsistencies by continuously adjusting settings without requiring complex control logic. The proposed mathematical model for the HE powerplant represents each component as a power node, where input power is transformed into output power according to the component's efficiency. A power balance equation ensures the congruence between input and output powers, reflecting the efficiency of each node. This kind of relation is represented in Eq. (4), where the number of input powers is represented by n, the number of output powers by k, $P_{In,j_{node}}$ is the jth input power value, $P_{Out,i_{node}}$ is the ith output power value, and η_{node} represents the component efficiency. Model linearity is preserved by assuming steady-state operation, constant efficiency, power balance at each node, and no transient behavior. Therefore, any power-dependent efficiency relation requires an iterative procedure (described later in this subsection) to calculate a stable power distribution.

$$\sum_{i=1}^{k} P_{Out,i_{node}} = \sum_{j=1}^{n} \left(P_{In,j_{node}} \cdot \eta_{node} \right) \tag{4}$$

To manage the power distribution along the two propulsion lines, the *shaft power ratio* (Φ) and the *thrust power ratio* (χ) are used. The *shaft power ratio* specifies the share of the total shaft power directed to the secondary shaft (Eq. (2)). In contrast, the *thrust power ratio* indicates the proportion of thrust force generated by the secondary propulsion line relative to the total thrust produced (Eq. (3)). These two parameters are interrelated, as described by Eq. (5), where η_{P_1} and η_{P_2} represent the efficiencies of the primary and secondary propulsion lines' propellers, respectively.

$$\Phi = \frac{\eta_{P_2}}{\eta_{P_1}} \left(\frac{\chi - 1}{\chi} \right) - 1 \tag{5}$$

Based on varying mission requirements, two distinct strategies have been developed to calculate power distribution across the component architecture: the *power source control strategy* and the *power required control strategy*.

Power source control strategy

The *power source control strategy* is effective for simulating powerplant behavior during specific flight segments where matching a precise

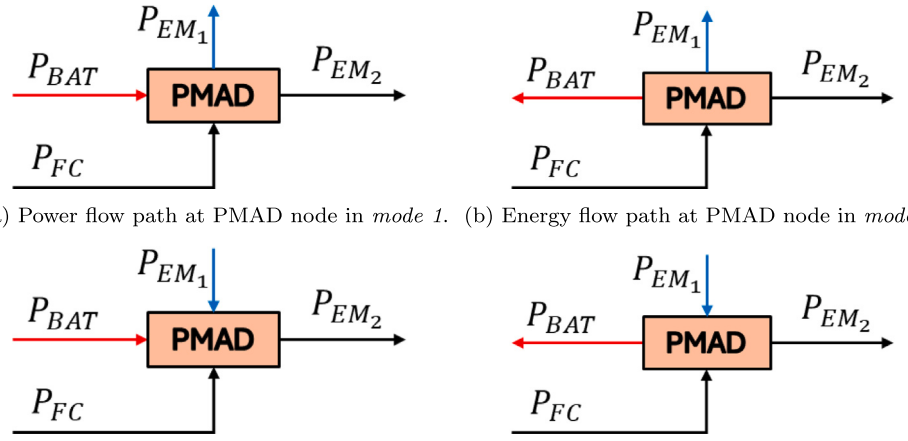

(a) Power flow path at PMAD node in *mode 1*. (b) Energy flow path at PMAD node in *mode 3*.

(c) Energy flow path at PMAD node in *mode 2*. (d) Power flow path at PMAD node in *mode 4*.

Fig. 2. Power flow distribution at the PMAD node for each possible *operation mode*.

power requirement is less critical, such as during take-off or constant-speed climb phases. This control strategy enables the designers to estimate the powerplant output power by selecting the power delivered from each power source. This is achieved by specifying the throttle settings for each power source ($\varphi_{GT}, \varphi_{FC}, \varphi_{BAT}$), a specific *operation mode*, and either a *shaft power ratio* or *thrust power ratio* value. By tracing the energy flow from the power sources to the propulsion lines, it is possible to estimate the power distribution across the architecture.

The process begins with the calculation of the power generated by each source (P_{GT}, P_{FC}, P_{BAT}) according to their throttle settings. By accounting for user-specified off-takes, the effective usable powers $P_{GT_{eff}}, P_{FC_{eff}}, P_{BAT_{eff}}$ are derived. To accurately distribute powers along the two propulsion lines, a linear system of two equations must be solved. This system links the power outputs of the electric machines P_{EM_1} and P_{EM_2} to the shaft powers P_{S_1} and P_{S_2} according to the selected Φ parameter. Solving this system enables the calculation of the total power flow within the architecture, including the mechanical shaft powers P_{S_1} and P_{S_2}, and the corresponding propulsive powers P_{P_1}, P_{P_2}, P_P. Fig. 2 illustrates the power flow paths at the PMAD node for each *operation mode*.

For each selected *operation mode*, a different system of equations must be solved, where the first equation ensures the power balance at the PMAD node according to the specified power flow path, while the second correlates the mechanical power on each shaft with the output from the electric machines as dictated by the Φ parameter. Eq. (6) details the system of equations that must be solved to describe the powerplant behavior within *mode 1*, where $\eta_{EM_1}, \eta_{GB_1}, \eta_{EM_2}, \eta_{GB_2}$, and η_{PMAD} denote the efficiencies of EM_1, GB_1, EM_2, GB_2, and PMAD respectively.

$$\begin{bmatrix} 1 & 1 \\ \eta_{EM_1} \cdot \eta_{GB_1} & -\eta_{GB_2} \cdot \eta_{EM_2} \cdot \dfrac{1-\Phi}{\Phi} \end{bmatrix} \begin{bmatrix} P_{EM_1} \\ P_{EM_2} \end{bmatrix} = \begin{bmatrix} \eta_{PMAD} \cdot (P_{FC_{eff}} + P_{BAT_{eff}}) \\ -P_{GT_{eff}} \cdot \eta_{GB_1} \end{bmatrix} \tag{6}$$

Fig. 3 provides a comprehensive overview of the procedure for calculating the power distribution across the HE architecture using the *power source control strategy*.

Power required control strategy

While the *power source control strategy* focuses on estimating the powerplant output based on user-defined throttle settings for the power sources, the *power required control strategy* is designed to meet specific power demand at the propulsion shafts. With this approach the designer specifies the desired power demand (P_P) along with the throttle settings for the electric sources (φ_{FC}, φ_{BAT}) and either the *shaft power ratio* or the *thrust power ratio*. From these parameters, the model automatically estimates the necessary gas turbine throttle setting (φ_{GT}) that satisfies the required power demand. This control strategy is particularly useful to simulate cruise flight segments or constant-speed at prescribed rate of descent (RD) descent phases, where a specific power request must be satisfied.

To estimate power distribution, the power flow must be traced from two starting points: the first originates from the electric power sources, and the second from the two propulsion shafts, where the required propulsive power (P_P) is specified.

The calculation begins by estimating the power produced by the electric sources (P_{FC} and P_{BAT}), which is converted into effective usable power ($P_{BAT_{eff}}$ and $P_{FC_{eff}}$) by accounting for auxiliary off-takes. From the specified power requirement P_P and the selected *shaft power ratio* Φ, the power values that must be guaranteed at both propulsive shafts (P_{S_1} and P_{S_2}) are calculated. From the secondary shaft power value obtained, the corresponding gearbox (P_{GB_2}) and electric machine (P_{EM_2}) power values are then determined. Based on the power balance at the PMAD node, the power output of the primary electric machine (P_{EM_1}) is calculated. This value is then used to estimate the gas turbine power (P_{GT}) and its corresponding throttle setting φ_{GT} required to meet the specific power demand.

Fig. 4 provides a detailed step-by-step mathematical workflow for estimating the power distribution within the powerplant for each *operation mode*.

Modeling of individual power sources and components

To ensure a straightforward and linear mathematical formulation suitable for the preliminary analysis of an HE powerplant model, a simplified approach must be adopted for modeling the power and efficiency of each sub-component within the architecture.

The gas turbine engine is modeled using a performance table (*engine deck*) that provides power output (P_{GT}), fuel flow (FF_{GT}), and emissions data across varying conditions of altitude (h), Mach number (M), temperature deviation (ΔT_{ISA}), and throttle setting (φ_{GT}) for different power ratings. Each rating represents the engine behavior pertinent to different mission phases and operating modes, namely take-off, flight idle, ground idle, max. continuous, auxiliary power reserve (APR), and cruise. By interpolating the data in the table, the performance of the thermal engine can be estimated. The fuel cell system (FC) is also modeled through a performance table allowing its output power (P_{FC}), hydrogen consumption (FF_{FC}), and emissions to be correlated with ambient and operating conditions. The efficiencies of these two power sources, denoted as η_{GT} and η_{FC}, are calculated using Eq. (7), which defines efficiency as the ratio of power produced to the product of fuel consumed and the fuel's specific energy (SE). SE represents the energy content per kilogram of fuel, with typical values of 12 kWh/kg

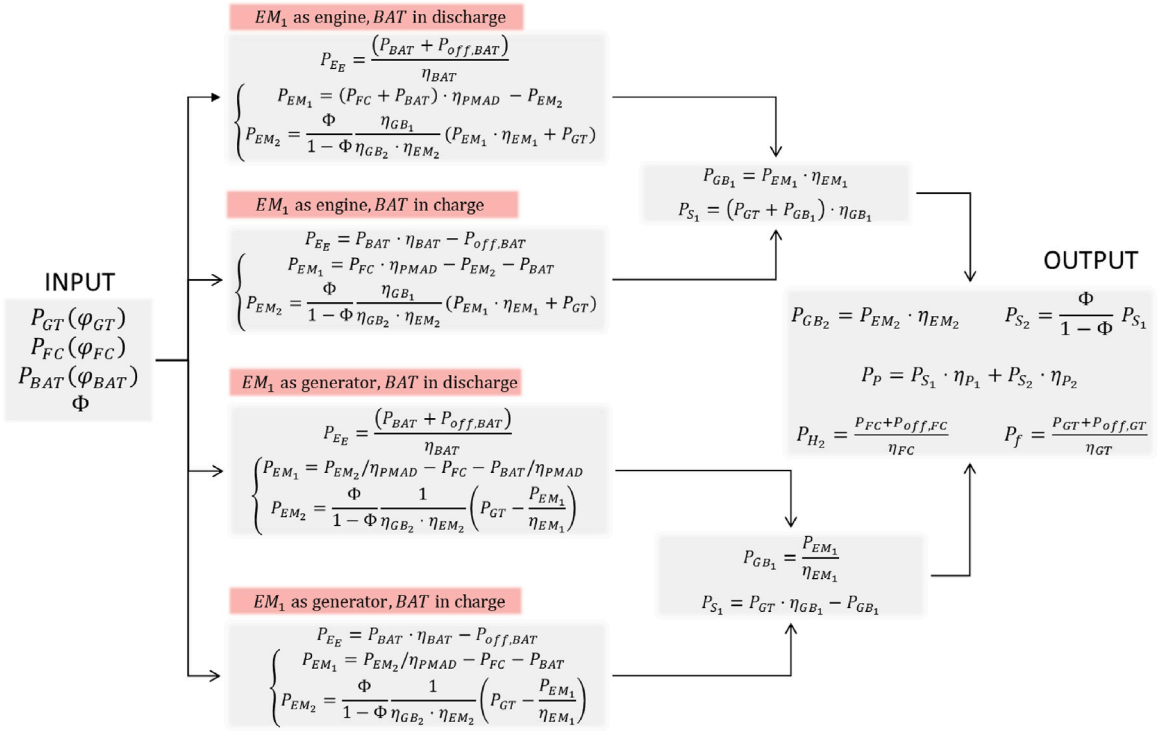

Fig. 3. HE powerplant mathematical model workflow using the *power source control strategy*.

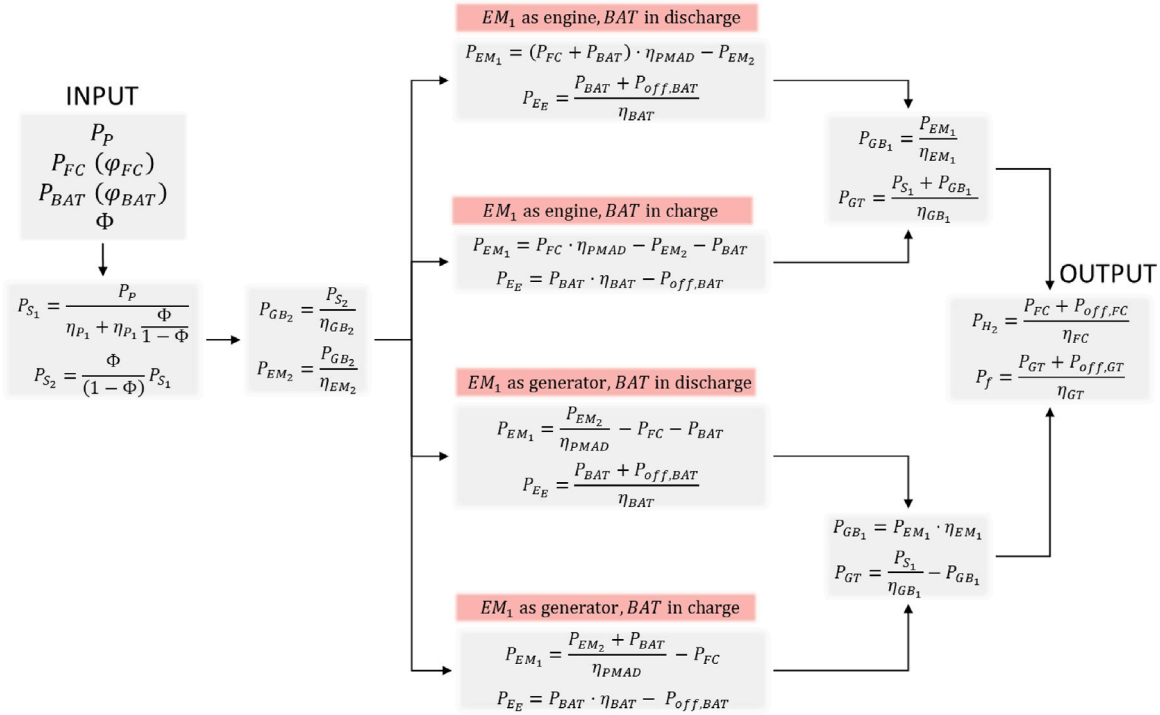

Fig. 4. HE powerplant mathematical model workflow using the *power required control strategy*.

for kerosene and 33 kWh/kg for hydrogen. Estimating the efficiencies of these two power sources requires interpolating the *engine deck* tables based on the specific mission parameters.

$$\eta = \frac{P(M, h, \Delta T, \varphi)}{FF(M, h, \Delta T, \varphi) \cdot SE} \tag{7}$$

The electric storage system (BAT) is characterized by its maximum capacity (total stored electric energy), maximum *C-Rate* (maximum charge or discharge rate), number of battery packs (n_{packs}), and a throttle parameter (φ_{BAT}). The power extracted or supplied by the battery system is expressed as a fraction of its maximum power ($P_{BAT_{\max}}$), which is calculated using Eq. (8). The throttle value (φ_{BAT}) represent this power fraction and is defined by Eq. (9).

$$P_{BAT_{\max}} = \text{C-rate}_{\max} \cdot \text{Pack Capacity}_{\max} \cdot n_{packs}. \tag{8}$$

$$\varphi_{BAT} = \frac{\text{C-Rate}}{\text{C-Rate}_{\max}} = \frac{P_{BAT}}{P_{BAT_{\max}}}. \tag{9}$$

The battery system's efficiency can either be set as a constant or derived from a table, which relates efficiency to the required *C-Rate* and state of charge (SOC).

The remaining architectural components, such as electric machines, gearboxes, PMAD, cables, and propellers, do not require detailed power models and instead rely solely on efficiency models. To streamline the efficiency modeling process for each component, the authors allow the designer to either specify a constant efficiency value or interpolate values from a user-defined table that relates the component's efficiency to its output power. The efficiency model for propellers differs slightly, offering the designer the option to use a constant efficiency value or estimate it iteratively using a modified Rankine–Froude model, depending on mission parameters as described in [47, p. 639].

Adopting power-dependent efficiency models requires iteratively refining the power distribution calculated using the two described control strategies until a stable solution is achieved. These iterations are necessary because the component efficiency directly depends on its power value and vice versa. To ensure convergence, the following iterative procedure has been implemented:

1. **Initialize efficiencies**: Assign initial constant efficiencies to all components.
2. **Calculate power distribution**: Solve for the power distribution using either the *power source control strategy* or the *power required control strategy*.
3. **Update efficiencies**: Recompute efficiencies based on the calculated power values.
4. **Recalculate power distribution**: Solve the power distribution again using updated efficiencies.
5. **Check for convergence**: Repeat steps 3 and 4 until changes in efficiency fall below a predefined threshold.

2.2. Powerplant management algorithm

The control strategies presented in Section 2.1 enable the estimation of power distribution across the architecture to meet various power requirements. However, inconsistencies may arise if the input data is incorrectly combined. For instance, in the *power source control strategy*, inconsistencies occur when the *operation mode*, *shaft power ratio*, and throttle settings fail to maintain power balance across each power node, resulting in physically inconsistent solutions. Similarly, in the *power required control strategy*, an improperly selected energy flow or insufficient throttle settings for electric sources may prevent the system from satisfying the requested power demand or yield non-physical solutions. To address these issues while preserving as much as possible of the designer's input, a straightforward power management algorithm has been developed, suitable for the preliminary analysis phase. This algorithm, compatible with both control strategies, ensures consistent and feasible solutions by adjusting input data and resolving power flow discrepancies without requiring complex control logic.

When the *power source control strategy* is used and a power flow inconsistency is detected, the algorithm adjusts the *operation mode* by switching the role of the primary electric machine while maintaining the specified battery role. Conversely, when using the *power required control strategy*, if the power request cannot be satisfied based on the selected input data, or if a power flow inconsistency is detected, the algorithm adjusts the power source throttle settings to meet the power demand. If necessary, it also modifies the *operation mode* to ensure a physically consistent solution.

The power management algorithm incorporates two specific operational settings to efficiently manage these adjustments:

- *Autofix battery throttle*: allows the algorithm to adjust the battery throttle to meet the required power demand.
- *Match with power off-takes*: manages any excess power output by dissipating it through additional power off-takes.

Table 2
Throttle combinations used by the power management algorithm to estimate characteristic powers, based on the role of electric storage. Here, $\varphi_{GT_{\min}}$ and $\varphi_{FC_{\min}}$ denote the minimum admissible throttle settings for the gas turbine and fuel cell system, respectively; $\varphi_{FC_{\text{in}}}$ and $\varphi_{BAT_{\text{in}}}$ are the user-selected throttle values for the electric sources; and φ^*_{BAT} represents the battery throttle value that satisfies the optimization problem described in Eq. (10).

Power value	Electric storage	φ_{GT}	φ_{FC}	φ_{GT}
$P_{\max}$	Discharge	1.0	1.0	1.0
$P_{\max}$	Charge	1.0	1.0	0.0
$P_{\min}$	Discharge	$\varphi_{GT_{\min}}$	$\varphi_{FC_{\min}}$	0.0
$P_{\min}$	Charge	$\varphi_{GT_{\min}}$	$\varphi_{FC_{\min}}$	φ^*_{BAT}
$P_{\min_{\text{eff}}}$	Whatever	$\varphi_{GT_{\min}}$	$\varphi_{FC_{\text{in}}}$	$\varphi_{BAT_{\text{in}}}$
$P_{\max_{\text{eff}}}$	Whatever	1.0	$\varphi_{FC_{\text{in}}}$	$\varphi_{BAT_{\text{in}}}$

The powerplant management algorithm operates using four key power values, $P_{\max}$, $P_{\min}$, $P_{\min_{\text{eff}}}$, and $P_{\max_{\text{eff}}}$, that define its feasible operating range. $P_{\max}$ and $P_{\min}$ represent the absolute power limits, while $P_{\max_{\text{eff}}}$ and $P_{\min_{\text{eff}}}$ correspond to maximum and minimum power that the powerplant can produce according to the user-selected throttle values. These characteristic power values can be estimated using the *power source control strategy* with the throttle combinations shown in Table 2, where each row indicates how the gas turbine, fuel cell, and battery throttles should be combined according to the electric storage's role. Here, $\varphi_{GT_{\min}}$ and $\varphi_{FC_{\min}}$ are the lowest admissible throttle settings for the gas turbine and fuel cell system, respectively, whereas $\varphi_{FC_{\text{in}}}$ and $\varphi_{BAT_{\text{in}}}$ represent the user-selected electric source throttle values. The battery's throttle setting, φ^*_{BAT}, is determined by solving the minimization problem outlined in Eq. (10), aiming to find the lowest feasible power output within these constraints. It is important to note that an incorrect combination of the *operation mode* and input data may prevent the successful calculation of $P_{\min_{\text{eff}}}$ and $P_{\max_{\text{eff}}}$.

$$\begin{aligned} \min_{\varphi_{BAT}} \quad & P_P(\varphi_{BAT}) \\ \text{s.t.} \quad & \varphi_{GT} = \varphi_{GT_{\min}}, \\ & \varphi_{FC} = \varphi_{FC_{\min}} \end{aligned} \tag{10}$$

Once these four power values are determined, the algorithm checks whether the user-requested power, P_{req}, is within the boundaries $P_{\min}$ and $P_{\max}$. If P_{req} falls outside these limits, the algorithm returns the closest boundary value. Otherwise, three sub-processes (labeled *A*, *B*, and *C*) adjust the throttles to meet the power demand. First, by modifying a single power source. Then, if necessary, by adjusting two of them simultaneously.

The adjustment of a single throttle is executed using a root-finding method, such as Brent's method [48], to minimize the L1 norm of the power error, denoted as $\|P_{\text{req}} - P(\varphi)\|_1$. Simultaneous adjustments of two throttles are achieved by minimizing the squared difference $(P_{\text{req}} - P(\varphi, \psi))^2$. Due to potential inconsistencies arising from various throttle combinations and *operation modes*, the authors did not use gradient-based methods. Instead, they employed the Nelder–Mead simplex method combined with grid-based sampling to solve this optimization problem. It is important to note that each power estimation was performed using the *power source control strategy*.

Figs. 5(a) and 5(b) illustrate these methodologies, referred to as *ST-Adjust* for single throttle adjustment and *DT-Adjust* for double throttle adjustment, respectively.

The three defined sub-processes are coordinated by the main powerplant management algorithm, as outlined in Algorithm 1, and all of them act to satisfy the power request by applying the two described adjustment strategies to different power sources.

Sub-process A (Algorithm 2) is executed when $P_{max_{eff}} \leq P_{req}$. This sub-process aims to meet the power demand based on the *autofix battery*

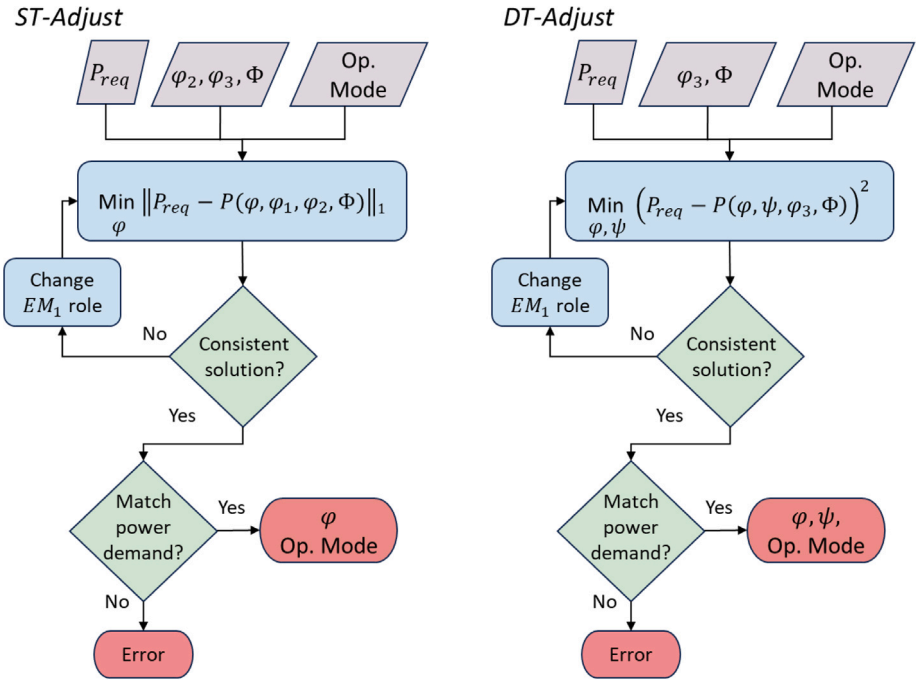

(a) Single throttle adjustment (ST-$Adjust$) block diagram.

(b) Double throttle adjustment (DT-$Adjust$) block diagram.

Fig. 5. Block diagram representations of the single (left) and double (right) throttle adjustment algorithms, used by the powerplant management algorithm.

Algorithm 1 Power Management Algorithm

Require: $P_{req}, \varphi_{FC}, \varphi_{BAT}, \Phi$, *operation mode*, *autofix battery throttle*, *match with power off-takes*, mission parameters.
Ensure: $P_P = P_{req}$
1: Estimate P_{max} and P_{min}
2: **if** $P_{min} \leq P_{req} \leq P_{max}$ **then**
3: Estimate $P_{max_{eff}}$ and $P_{min_{eff}}$
4: **if** ($P_{min_{eff}}$ is null) **and** ($P_{max_{eff}}$ is not null) **then**
5: $P_{min_{eff}} \leftarrow P_{max_{eff}}$
6: **end if**
7: **if** $P_{max_{eff}} \leq P_{req}$ **then**
8: Execute *sub-process A*
9: **end if**
10: **if** $P_{min_{eff}} \geq P_{req}$ **then**
11: Execute *sub-process B*
12: **end if**
13: **if** ($P_{max_{eff}}$ is null) **and** (P_{req} is null) **then**
14: Execute *sub-process C*
15: **end if**
16: **else**
17: **return** P_{max} or P_{min}
18: **end if**

Algorithm 2 Sub-process A algorithm

Require: $P_{req}, \varphi_{FC_{in}}, \varphi_{BAT_{in}}, \tilde{\varphi_{GT}}, \Phi$, *operation mode*, *autofix battery throttle*, *match with power off-takes*, mission parameters.
Ensure: $P_P = P_{req}$
1: **if** *autofix battery throttle* **then**
2: $P_p, \varphi_{BAT} \leftarrow$ *ST-Adjust* for BAT .
3: **if** $P_P \neq P_{req}$ **then**
4: $P_p, \varphi_{BAT}, \varphi_{FC} \leftarrow$ *DT-Adjust* for BAT and FC .
5: **end if**
6: **else**
7: $P_p, \varphi_{FC} \leftarrow$ *ST-Adjust* for FC.
8: **end if**
9:
10: **if** $P_P = P_{req}$ **then**
11: **return** $P_P, \varphi_{BAT}, \varphi_{FC}, \varphi_{GT}$
12: **else**
13: **return** $P_{max_{eff}}$
14: **end if**

throttle setting. If this setting is enabled, the algorithm first applies the *ST-Adjust* method to the battery. If this adjustment fails to find a solution, the algorithm then implements a *DT-Adjust* strategy, which involves both the battery and the fuel cell. When the *autofix battery throttle* is disabled, the *ST-Adjust* strategy is applied to satisfy the power request by changing the fuel cell throttle. If no solution is found, the algorithm prompts the user to either adjust the battery throttle value or activate the *autofix battery throttle* setting, ultimately returning the $P_{max_{eff}}$ value. In Algorithm 2, $\tilde{\varphi}_{GT}$ represents the gas turbine throttle value selected to evaluate $P_{max_{eff}}$ value (see Table 2).

Sub-process B (Algorithm 3) is activated when $P_{min_{eff}} \geq P_{req}$. This sub-process first evaluates the *autofix battery throttle* setting. If this feature is enabled, the algorithm begins by modifying the battery throttle. If the desired outcome is not achieved, it applies a *DT-Adjust* to both the battery and the fuel cell. If the setting is disabled, the adjustments start with the gas turbine throttle and, if it is not sufficient, extend to a *DT-Adjust* including the fuel cell throttle. If the algorithm still does not meet the power request after applying these strategies, it considers whether to dissipate the excess power through additional off-takes or simply return $P_{min_{eff}}$, depending on the *match with power off-takes* setting. In Algorithm 3, $\hat{\varphi}_{GT}$ denotes the gas turbine throttle for $P_{min_{eff}}$, as detailed in Table 2.

Sub-process C (Algorithm 4) is adopted when neither $P_{max_{eff}}$ nor $P_{min_{eff}}$ can be successfully calculated. This situation occurs when the battery, operating in charge mode, demands more power than can

Algorithm 3 Sub-process B algorithm

Require: $P_{req}, P_{min_{eff}}, \varphi_{FC_{in}}, \varphi_{BAT_{in}}, \hat{\varphi_{GT}}, \Phi$, *operation mode*, *autofix battery throttle*, *match with power off-takes*, mission parameters.
Ensure: $P_P = P_{req}$
1: **if** *autofix battery throttle* **then**
2: $P_p, \varphi_{BAT} \leftarrow$ *ST-Adjust* for BAT
3: **if** $P_P \neq P_{req}$ **then**
4: $P_p, \varphi_{BAT}, \varphi_{FC} \leftarrow$ *DT-Adjust* for BAT and FC
5: **end if**
6: **else**
7: $P_p, \varphi_{GT} \leftarrow$ *ST-Adjust* for GT
8: **if** $P_P \neq P_{req}$ **then**
9: $P_p, \varphi_{GT}, \varphi_{FC} \leftarrow$ *DT-Adjust* for GT and FC
10: **end if**
11: **end if**
12: **if** $P_P \neq P_{req}$ **then**
13: **return** $\varphi_{GT}, \varphi_{BAT}, \varphi_{FC}$
14: **else if** *match with power off-takes* **and** $P_{min_{eff}} > P_{req}$ **then**
15: $P_{GT,off}, P_{FC,off}, P_{BAT,off} \leftarrow$ Find additional off-takes
16: **return** $P_{off,GT}, P_{off,FC}, P_{off,BAT}$
17: **else**
18: **return** $P_{min_{eff}}$
19: **end if**

be supplied by the combined maximum (or minimum) outputs of the gas turbine and the fuel cell. Due to the high power demand from the battery, the gas turbine throttle remains at its maximum setting throughout this sub-process. If *autofix battery throttle* is enabled, a single-throttle adjustment (*ST-Adjust*) is executed on the battery to decrease its power requirement. Conversely, if *autofix battery throttle* is disabled, the algorithm computes P_p^*, which is the maximum power achievable by combining the selected battery throttle with the highest outputs from both the gas turbine and the fuel cell. If $P_p^* > P_{req}$, an appropriate fuel cell throttle can be determined using *ST-Adjust*. If this condition is not met, it becomes necessary to reduce the battery's power demand to satisfy P_{req}, thereby automatically activating the *autofix battery throttle* to ensure a consistent solution.

Algorithm 4 Sub-process C algorithm

Require: $P_{req}, \varphi_{FC_{in}}, \varphi_{BAT_{in}}, \Phi$, *operation mode*, *autofix battery throttle*, *match with power off-takes*, mission parameters.
Ensure: $P_P = P_{req}$
1: $\varphi_{GT} \leftarrow 1.0$
2: $P_p^* \leftarrow$ *power source control strategy*$(\varphi_{GT}, \varphi_{FC} = 1.0, \varphi_{BAT} = \varphi_{BAT_{In}}, \Phi)$
3: **if not** *autofix battery throttle* **then**
4: **if** $P_p^* < P_{req}$ **then**
5: *autofix battery throttle* $\leftarrow$ True
6: **end if**
7: **end if**
8: **if** *autofix battery throttle* **then**
9: $P_p, \varphi_{BAT} \leftarrow$ *ST-Adjust* for BAT
10: **else**
11: $P_p, \varphi_{FC} \leftarrow$ *ST-Adjust* for FC
12: **end if**
13: **if** $P_p = P_{req}$ **then**
14: **return** $\varphi_{GT}, \varphi_{BAT}, \varphi_{FC}$
15: **else**
16: **return** Error
17: **end if**

In summary, this powerplant management algorithm effectively addresses the complexities and potential inconsistencies in HE powerplant control strategies. By leveraging adaptive sub-processes and incorporating both single and dual-throttle adjustment techniques, it successfully satisfies power demands while maintaining physically consistent solutions. Operational settings such as *autofix battery throttle* and *match with power off-takes* enable designers to customize the powerplant responses meeting specific needs, thereby enhancing the adaptability of the model. This method, suitable for preliminary analysis, establishes a robust framework to analyze the behavior of a preliminary sized HE powerplant, allowing the designer to understand what is the best power source combination that could be used to satisfy a specific assigned power requirement.

Table 3
Test cases summary. All cases assume that the first propulsion line electric motor (EM_1) operates as a motor and the battery (BAT) is in discharge mode.

Test Case	*Autofix battery throttle*	Φ	Case IDs
CASE 1	True	0.0	1 – 1 1 – 2 1 – 3 1 – 4 1 – 5
CASE 2	False	0.0	2 – 1 2 – 2 2 – 3
CASE 3	True	0.5	3 – 1 3 – 2

Table 4
Characteristics of the gas turbine engine, fuel cell, and battery systems adopted for the hybrid-electric powerplant used in the mathematical model demonstration.

Element	Number	Description
Gas turbine engine	2	$P_{GT} = \varphi_{GT} \cdot P_{GT_{max}}$, where $P_{GT_{max}} = 2500\,\text{kW}$
Fuel cell system	2	$P_{FC} = \varphi_{FC} \cdot P_{FC_{max}}$, where $P_{FC_{max}} = 1000\,\text{kW}$
Battery system	2	Maximum capacity of 300 kWh with C-Rate$_{max}$ = 2.5 1/h

3. Case studies

3.1. Powerplant model mathematical demonstration

The proposed HE powerplant model enables designers to evaluate a powerplant that integrates up to three distinct power sources, supporting preliminary studies of a HE propeller-driven aircraft. As discussed in Section 2, combining the proposed powerplant control strategies with the powerplant management algorithm (Section 2.2) yields a flexible model that ensures physically consistent solutions while adhering closely to the designer's input requirements.

In the following, three test cases assess the powerplant's capability to meet varying power demands while ensuring physically consistent operation. They differ in *autofix battery throttle* settings and *shaft power ratio* Φ. Each test case includes multiple case IDs, representing distinct power requests (Table 3).

CASE 1 depicts conditions in which EM_1 operates as a motor and the electric storage is in discharge mode, with *autofix battery throttle* enabled and $\Phi = 0.0$. Under these settings, the powerplant must provide the requested power using only the primary propulsion line. Five different power requests (five case IDs) illustrate how the powerplant reacts under this configuration. *CASE 2* uses the same power requests as *CASE 1* but disables the *autofix battery throttle* setting, thereby showing how removing this option influences the algorithm's ability to fulfill the requested power. Finally, *CASE 3* demonstrates how the powerplant satisfies power demands by using the same operational settings as *CASE 1* but requesting $\Phi = 0.5$, distributing the required power equally across the two propulsion lines.

Table 5
Constant efficiency values assumed for each hybrid-electric powerplant sub-component.

Powerplant element	Value
Gas turbine	0.30
Fuel cell system	0.40
Battery system	0.95
Cables system	1.00
PMAD system	0.99
Primary electric machine	0.96
Primary gearbox	0.97
Primary propeller	0.85
Secondary electric machine	0.95
Secondary gearbox	0.95
Secondary propeller	0.83

The HE powerplant architecture analyzed in this case study is powered by three energy sources, as outlined in Table 4, and integrates two distinct propulsion lines. For simplicity, each sub-component is characterized by a constant efficiency value, detailed in Table 5.

Before analyzing the powerplant's responses, it is useful to consider the key power values calculated for the operation settings defined for *CASE 1* and *CASE 2* (Table 3). These values, namely $P_{min} = 570\,\text{kW}$, $P_{min_{eff}} = 1587\,\text{kW}$, $P_{max} = 6867\,\text{kW}$, and $P_{max_{eff}} = 5300\,\text{kW}$, represent the lower and upper operational power limits, as well as their "effective" counterparts under the specified operating conditions. Table 6 summarizes, for each case ID, the required power, the produced power, the estimated source throttles, and whether the *operation mode* needs to be modified. NA (Not Applicable) indicates that, when using the *power required control strategy*, the φ_{GT} value does not need to be assigned.

In *CASE 1*, IDs 1-1, 1-2, and 1-3, the power request decreases but remains within acceptable operating ranges. For ID 1-1, since $P_{max_{eff}} < P_{req}$, *sub-process A* increases both the electric source throttles to meet the power demand. For ID 1-3, where $P_{min_{eff}} > P_{req}$, *sub-process B* reduces both electric source throttles, as lowering only the battery throttle is insufficient. ID 1-2 remains within the power boundaries and does not require intervention by the powerplant management algorithm. IDs 1-4 and 1-5 illustrate scenarios where the power requests lie beyond the operational range; the powerplant model therefore returns the closest achievable power level.

In *CASE 2*, IDs 2-1, 2-2, and 2-3, the *autofix battery throttle* is disabled, altering how the model addresses power requests previously handled in *CASE 1*. For ID 2-1, *sub-process A* cannot satisfy the power demand without adjusting the battery throttle, so the algorithm settles on $P_{max_{eff}}$. By contrast, the power request in ID 2-3 is met by *sub-process B*, which adjusts only the fuel cell throttle. ID 2-2 behaves like ID 1-2, as the required power remains within bounds, making further adjustments unnecessary.

CASE 3 sets $\Phi = 0.5$, requiring equal power distribution across both propulsion lines. None of the case IDs within *CASE 3* require the power management algorithm to fulfill the request, although they highlight the importance of switching the *operation mode* to preserve physical consistency. Increasing gas turbine power while maintaining $\Phi = 0.5$ may require transitioning from *mode 1* (EM_1 acting as motor) to *mode 3* (EM_1 acting as generator). Fig. 6 shows the minimum battery throttle (φ_{BAT}) needed to preserve *mode 1*. If the system drops below this threshold, it must change to *mode 3*, thereby assigning a generator role to the primary electric machine. Specifically, for IDs 3-1 and 3-2, the figure indicates battery throttle thresholds of $\varphi_{3-1} = 0.48$ and $\varphi_{3-2} = 0.0$. These values reveal that *mode 1* remains valid for ID 3-2 at any battery throttle value, as $0.2 > \varphi_{3-2}$. However, ID 3-1 must switch to *mode 3* to maintain a physically consistent solution, because $0.2 < \varphi_{3-1}$.

A graphical representation of nonphysical and physical solutions for CASE 3-1 appears in Fig. 7. Fig. 7(a) shows the nonphysical behavior resulting from an imbalance of power at the PMAD node while still

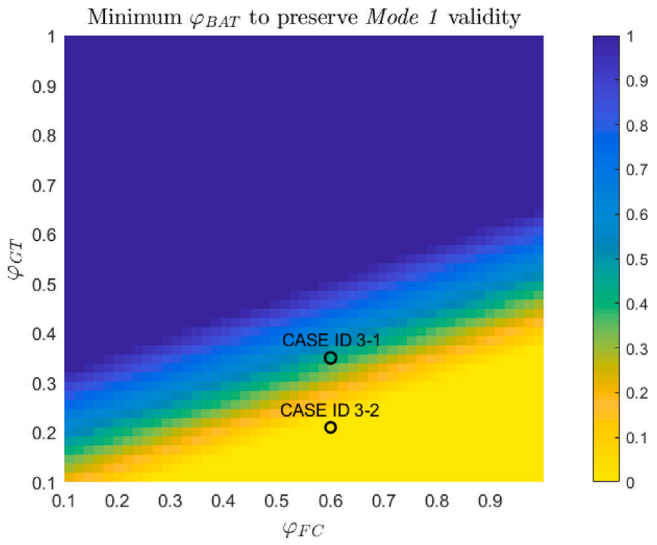

Fig. 6. Minimum φ_{BAT} value map to preserve *mode 1* physical consistency. Throttle values below this limit indicate the need to change the selected operation mode, switching from *mode 1* to *mode 3* and inverting the EM_1 role from motor to generator.

operating in *mode 1*. Switching to *mode 3* enables CASE ID 3-1 to reach a consistent solution, as depicted in Fig. 7(b).

A relationship among the three power sources that leads to nonphysical behavior in *mode 1* can also be derived. According to Eq. (4), a nonphysical state arises if at least one node of the powerplant fails to satisfy the power balance requirement. When the balance is not met, some power element within the architecture takes on a negative value. When applying the *power source control strategy* the PMAD node is the critical node from which the power inconsistency could arise, and the critical elements linked to it are the electric machines. Therefore, determining when *mode 1* ceases to be physical involves identifying when the electric machines' power switches sign. By solving the system given in Eq. (6), the electric machines' powers can be estimated in terms of the remaining powerplant parameters (Eq. (11)).

$$\begin{cases} P_{EM_1} = \dfrac{(P_{FC}+P_{BAT})\eta_{GB_2}\cdot\eta_{EM_2}\cdot\eta_{PMAD}(1-\Phi)-\Phi\cdot P_{GT}\cdot\eta_{GB_1}}{\eta_{GB_2}\cdot\eta_{EM_2}(1-\Phi)+\eta_{EM_1}\cdot\eta_{GB_1}\cdot\Phi} \\ P_{EM_2} = \dfrac{(P_{FC}+P_{BAT})\Phi\cdot\eta_{EM_1}\cdot\eta_{GB_1}\cdot\eta_{PMAD}+P_{GT}\cdot\eta_{GB1}\cdot\Phi}{\eta_{GB_2}\cdot\eta_{EM_2}(1-\Phi)+\eta_{EM_1}\cdot\eta_{GB_1}\cdot\Phi} \end{cases} \tag{11}$$

From this set of equations, the condition that preserves *mode 1* emerges (Eq. (12)). Under constant efficiency assumptions and $0 \le \Phi < 1.0$, the total electric power produced by the two electric sources must be larger than the power from the thermal engines multiplied by an amplification factor. Applying this to CASE ID 3-1 and 3-2 reveals the maximum gas turbine throttle value that preserves the *mode 1* consistency. Exceeding this value, as in ID 3-1, leads to the nonphysical behavior described earlier. The calculated throttle limit is $\varphi_{GT} = 0.27$.

$$(P_{FC}+P_{BAT}) \ge P_{GT}\cdot\left(\frac{\Phi}{1-\Phi}\right)\left(\frac{\eta_{GB_1}}{\eta_{GB_2}}\right)\left(\frac{1}{\eta_{EM_2}\cdot\eta_{PMAD}}\right) \tag{12}$$

This analysis demonstrates how the powerplant model manages and satisfies different power requests under varying *shaft power ratios* and *autofix battery throttle* settings. The case studies illustrate how the model's management sub-processes enhance flexibility, providing physically consistent solutions that meet the designer's power requirements as closely as possible. Because of its simple mathematical formulation and basic power management controller, the proposed powerplant model is well suited for preliminary analyses of HE powerplant architectures.

Table 6
Powerplant behavior for the assigned case IDs power request. NA stands for Not Applicable and it is indicated because, when using the *power required control strategy*, the gas turbine throttle (φ_{GT}) value does not need to be assigned.

ID	Required power [kW]	Available power [kW]	Gas turbine		Fuel cell		Battery		Operation mode changed
			In	Out	In	Out	In	Out	
1–1	6500	6500	NA	1.00	0.60	1.0	0.20	0.69	false
1–2	3500	3500	NA	0.56	0.60	0.60	0.20	0.20	false
1–3	1000	1000	NA	0.10	0.60	0.30	0.20	0.10	false
1–4	8000	6867	NA	1.00	0.60	1.00	0.20	1.00	false
1–5	300	570	NA	0.10	0.60	0.10	0.20	0.00	false
2–1	6500	5300	NA	1.00	0.60	0.60	0.20	0.20	false
2–2	3500	3500	NA	0.56	0.60	0.60	0.20	0.20	false
2–3	1000	1000	NA	0.10	0.60	0.22	0.20	0.20	false
3–1	2500	2500	NA	0.35	0.60	0.60	0.20	0.20	true
3–2	2000	2000	NA	0.21	0.60	0.60	0.20	0.20	false

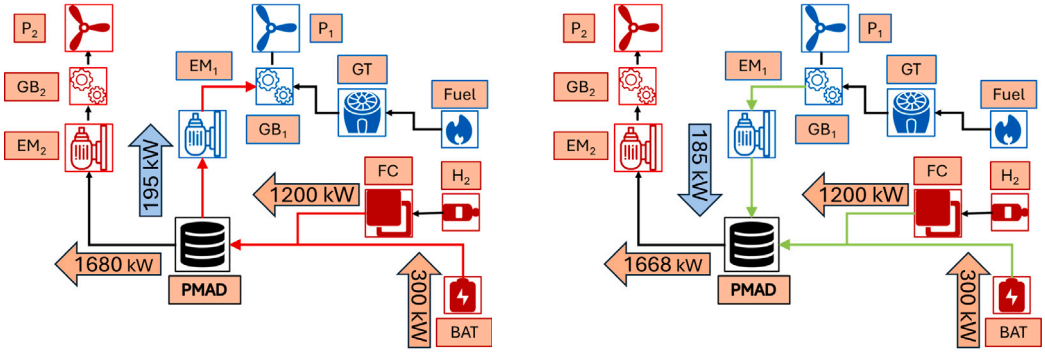

(a) Nonphysical power distribution for CASE ID 3-1, when EM_1 is forced to operate as a motor. This behavior produces an imbalance of power at the PMAD node.

(b) Correct power distribution for CASE ID 3-1 after switching the EM_1 role to generator. This change preserves the power balance at the PMAD node.

Fig. 7. Power distribution for CASE ID 3-1 before (a) and after (b) changing EM_1's role to achieve a physically consistent solution.

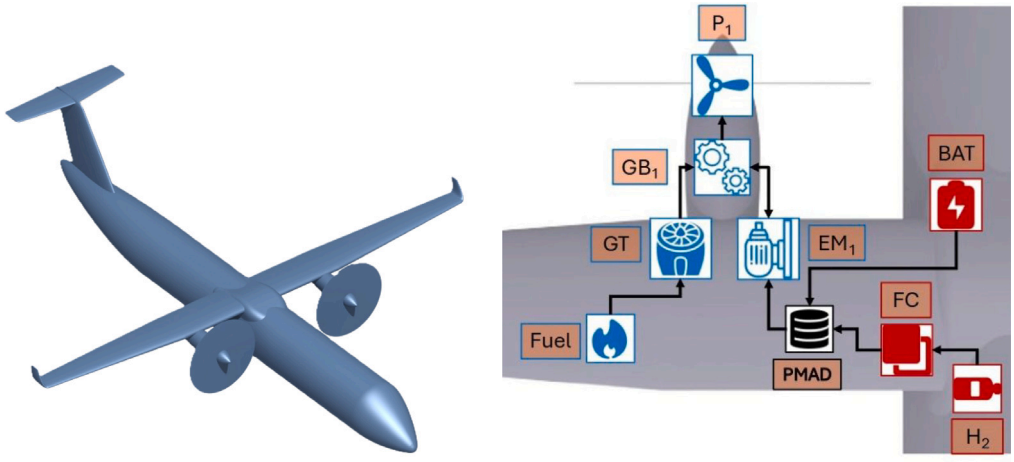

(a) Geometric 3D model of the 90-passenger hybrid-electric regional aircraft.

(b) Assumed powerplant architecture of the 90-passenger hybrid-electric regional aircraft.

Fig. 8. Geometry and powerplant architecture representations of the 90-passenger hybrid-electric regional aircraft. The left image illustrates the aircraft's geometric 3D model, highlighting key structural components and aerodynamic features. The right image details the assumed powerplant architecture, showcasing the integration of a three-source hybrid-electric system comprising a thermal engine, a fuel cell system, and a battery pack.

3.2. Aircraft application

The previous subsection demonstrated the theoretical powerplant model's capability to meet specific power requirements while ensuring physically feasible solutions. To illustrate the practical utility of the proposed methodology, the developed powerplant model was applied to assess the contribution of each power source during the cruise phase of a preliminarily sized HE regional aircraft. The aircraft sizing was performed using a proprietary, in-house developed tool, ensuring alignment with the top-level aircraft requirements (TLARs) presented in Table 7, which were derived from those of the Clean Aviation HERA research project [49]. The resulting aircraft, with a projected entry into service in 2035 and shown in Fig. 8(a), features a three-source HE powerplant architecture comprising a thermal engine, a fuel cell system,

Table 7
Top-level aircraft requirements for the regional propeller-driven aircraft selected for the powertrain model application. Climb performance values are intended with all engines operative. MTOM is the aircraft maximum take-off mass. FL indicates the flight level (*e.g.*, FL250 corresponds to 25 000 ft). KTAS represents the aircraft's true airspeed in knots.

Description	Value	Unit	Note
Entry into service	2035		
Design range	600	nmi	
Number of passengers	90		
Design payload	8550	kg	90 passengers @95 kg
Max payload	9000	kg	450 kg allowance mass
Take-off field length	≤ 1400	m	
Landing field length	≤ 1400	m	
Cruise speed	300	KTAS	FL250
Time to climb	≤ 20	min	@MTOM from FL15 to FL250
Reserves			100 nmi diversion, 30 min holding, 5% trip fuel

Table 8
Key geometrical, inertia, and performance characteristics of the 90-passenger hybrid-electric regional aircraft. SL denotes sea-level performance. ISA refers to standard day conditions (288.15 K). Climb performance values are calculated with all engines operative. FL indicates the flight level (*e.g.*, FL250 corresponds to 25 000 ft). KTAS represents the aircraft's true airspeed in knots.

Aircraft data	Value
Number of passengers	90
Wing area	75 m^2
Wing aspect ratio	14
Maximum Take-Off Mass (MTOM)	34 800 kg
Operative Empty Mass (OEM)	24 750 kg
Aircraft key performances	
Take-off field length @MTOM, SL, ISA	1360 m
Absolute ceiling @95% MTOM ISA	FL300
Time to climb from FL15 to FL250 @MTOM, ISA	18 min
Cruise altitude	25 000 ft
Cruise speed @FL250	300 KTAS
Landing field length @97% MTOM, SL, ISA	1300 m

and a battery pack, all supporting a single propulsive line. Fig. 8(b) provides a comprehensive overview of the powerplant configuration, while the key characteristics of this propeller-driven regional aircraft are summarized in Table 8.

Furthermore, Table 9 presents detailed data on the HE powerplant configuration, including the efficiencies assumed for the assigned flight mission. The performance table used to model the thermal engine was developed by scaling an in-house generated engine deck, based on a PW127-like engine (*i.e.*, the gas turbine engine installed on the ATR 42/72 aircraft's family), to the required sizing power. During the scaling process, the original relationships between shaft power and specific fuel consumption were preserved concerning key operating conditions, including thermal engine throttle setting, Mach number, altitude, and ambient temperature. Additionally, the specific fuel consumption values were adjusted to align with the aircraft's projected entry into service. In particular, a target value of 0.213 kg/kWh for specific fuel consumption under cruise conditions — defined by maximum power, Mach 0.50, and a flight altitude of 25 000 ft — was achieved. This target represents an improvement of approximately 20% compared to current typical values for regional propeller-driven aircraft. Subsequently, all specific fuel consumption values in the engine deck were scaled accordingly to maintain consistency across operating conditions.

The cruise phase analyzed corresponds to a 300 nmi typical mission, based on the mission profile illustrated in Fig. 9. The take-off and climb phases are computed using the *power source control strategy*, as these segments do not impose specific power constraints. In contrast, the descent and landing phases, which require maintaining a prescribed rate of descent, and cruise phase, performed at constant speed, are evaluated using the *power source control strategy* in conjunction with the developed *powerplant management algorithm*. Accordingly, Table 10 outlines the flight requirements for each phase, along with the corresponding throttle settings assigned to each power source. It is important to note that no throttle parameters are reported for the cruise phase, as the analysis focuses on the powerplant characteristics during this segment; therefore, a to be determined (TBD) value is indicated in the table. Conversely, not applicable (NA) denotes that the gas turbine throttle setting (φ_{GT}) is not required when the *power source control strategy* is applied. Additionally, the *autofix battery throttle* setting remains enabled throughout the mission, ensuring that the electric motor operates exclusively in motor mode.

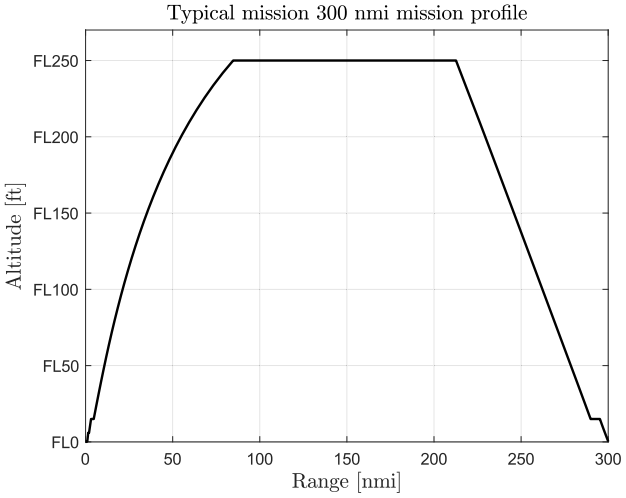

Fig. 9. Mission profile for a typical, 300 nmi flight. FL denotes the flight level (*e.g.*, FL250 corresponds to 25 000 ft).

To assess the impact of the different power sources on the aircraft's cruise performance, an analysis was conducted to determine the required gas turbine throttle setting (φ_{GT}) necessary to satisfy the cruise power demand, based on the assigned fuel cell and battery throttle settings ($\varphi_{FC-\text{Cruise}}$ and $\varphi_{BAT-\text{Cruise}}$). Fig. 10 illustrates the relationship between these assigned throttle values and that related to the thermal engine. Additionally, Fig. 11 presents the total energy required to complete the assigned mission, while Fig. 12 shows the total CO_2 emissions associated with the mission, both expressed as functions of the cruise phase electric power source throttle settings ($\varphi_{FC-\text{Cruise}}$ and $\varphi_{BAT-\text{Cruise}}$).

The two charts indicate that the combination of electric source throttle settings that minimizes the total mission energy requirement is achieved when the battery operates at full power, while the fuel cell operates at half of its maximum output power. Under these conditions, the corresponding gas turbine throttle setting that minimizes the total mission energy demand is $\varphi_{GT} = 0.7$. This optimal throttle combination reduces the total required energy primarily due to the lower hydrogen consumption associated with the fuel cell's reduced output power. Conversely, the minimum kerosene consumption — corresponding to the lowest total CO_2 emissions — is observed when both the fuel cell and battery systems operate at full power, thereby requiring the lowest gas turbine throttle setting.

This aircraft application illustrates how the proposed powerplant model assists designers in understanding how a preliminarily sized powerplant can operate to meet specific power requirements while consistently ensuring feasible solutions. Additionally, this application demonstrates how the model supports designers in identifying the optimal throttle settings to achieve specific objectives, such as minimizing total required energy or reducing CO_2 emissions.

Table 9
Powerplant characteristics of the 90-passenger hybrid-electric regional aircraft. The reported values represent the maximum power outputs of the energy sources and the component efficiency values assumed throughout the prescribed mission profile.

Powertrain element	Description
Gas turbine engine	Two thermal engines, each providing a maximum power output of 2550 kW. Specific fuel consumption in typical cruise condition equal to 0.213 kg/kWh.
Fuel cell system	Two fuel cell systems, each delivering a maximum power output of 1500 kW. System level efficiency at peak power equal to 55%.
Battery system	Two battery systems with a maximum capacity of 300 kWh each and a maximum discharge rate of C-Rate$_{max}$ = 0.7 1/h. Efficiency is set at 96%.
Electric machine	The assumed overall efficiency, including converter losses, is $\eta_{EM} = 0.93$ for the entire flight mission.
Reduction gearbox	The assumed gearbox efficiency is $\eta_{GB} = 0.98$ for the entire flight mission.
Propeller	The assumed propeller efficiency values are: $\eta_P = 0.82$ for cruise, $\eta_P = 0.85$ for climb and descent, and $\eta_P = 0.88$ for take-off.

Table 10
Assigned requirements and input throttle settings for each flight phase in the 300 nmi mission profile. NA (not applicable) indicates that the gas turbine throttle setting is not required when the *power source control strategy* is applied. TBD (to be determined) denotes that the cruise phase throttles will be varied during the analysis. SL represents sea-level altitude. CAS refers to calibrated airspeed, while TAS indicates true airspeed. RD denotes the rate of descent. FL represents the flight level (*e.g.*, FL250 corresponds to 25 000 ft).

Mission phase	Requirements	Gas turbine throttle	Fuel cell throttle	Battery throttle
Take-off	SL airport	1.0	1.0	0.0
Climb	Constant CAS speed schedule @190 KCAS from FL15 to FL250	1.0	1.0	0.0
Cruise	Constant altitude and TAS @FL250 and 300 KTAS	TBD	TBD	TBD
Descent	Constant CAS speed schedule and RD @220 KCAS and 1500 ft/min to FL15	NA	0.2	0.0
Landing	SL airport	NA	0.2	0.0

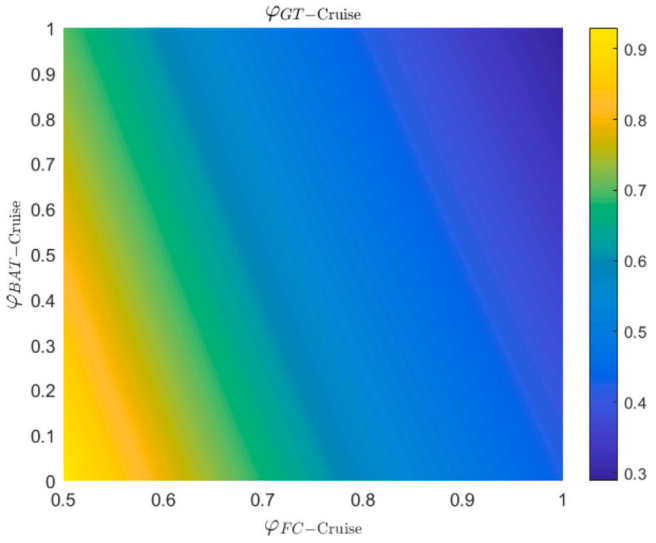

Fig. 10. Surface plot illustrating the gas turbine throttle setting ($\varphi_{GT-\text{Cruise}}$) required to meet the cruise power demand, based on the assigned fuel cell ($\varphi_{FC-\text{Cruise}}$) and battery ($\varphi_{BAT-\text{Cruise}}$) throttle settings. The gas turbine throttle values are estimated using the *power required control strategy*.

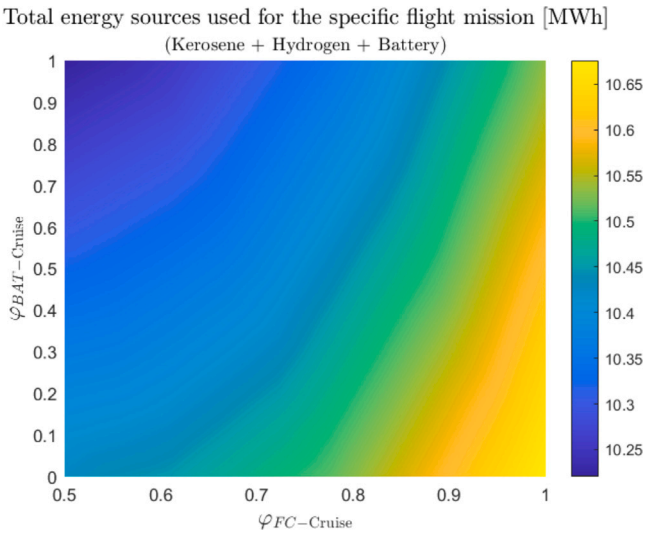

Fig. 11. Surface plot illustrating the total energy required from all power sources to complete the 300 nmi typical mission. The plot is presented as a function of the selected fuel cell ($\varphi_{FC-\text{Cruise}}$) and battery ($\varphi_{BAT-\text{Cruise}}$) throttle settings selected for the cruise phase.

4. Conclusion and future work

This work has introduced a three-source hybrid-electric powerplant model tailored for the preliminary performance analysis of hybrid-electric propulsion systems for propeller-driven aircraft. By employing a simple mathematical formulation and simplified component representations, the proposed powerplant model enables rapid evaluation of power distribution within the architecture, allowing designers to estimate the impact of each power source on overall power delivery.

Two different control strategies have been developed to operate with the proposed model: the *power source control strategy*, which calculates the powerplant's produced power based on user-defined

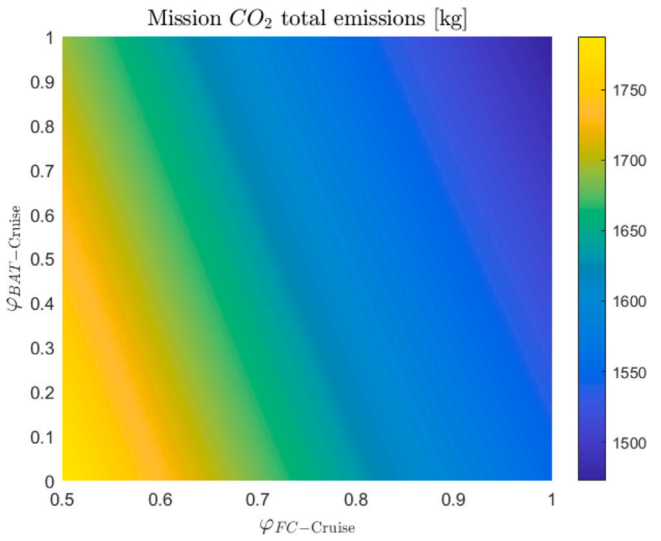

Fig. 12. Surface plot illustrating the total CO_2 emissions generated during the 300 nmi typical mission, presented as a function of the fuel cell ($\varphi_{FC-\text{Cruise}}$) and battery ($\varphi_{BAT-\text{Cruise}}$) throttle setting combinations selected for the cruise phase.

source settings, and the *power required control strategy*, which determines the gas turbine power level required to meet a specified power demand. These strategies help to quickly assess the behavior of an already sized powerplant, assisting the designer in understanding how it can be operated to satisfy specific power requirements. To ensure physically consistent solutions and solve potential power flow inconsistencies, a dedicated *powerplant management algorithm* was implemented. This algorithm adjusts the power source throttle settings and, if necessary, modifies the selected *operation mode* to deliver the required power while maintaining a consistent power distribution across the architecture. As a result, when combined with the proposed control strategies, the powerplant model can identify and resolve power path inconsistencies, thereby avoiding nonphysical power distributions. Although not designed to provide optimal real-time energy management solutions, the *powerplant management algorithm* is robust enough to rapidly evaluate power distributions and identify potential sizing limitations. It is also flexible enough to satisfy selected power requirements, closely adhering to the designer's needs, and provides clear feedback if user-defined settings lead to nonphysical outcomes.

To demonstrate the capabilities of the developed powerplant model, two primary applications have been analyzed and presented. The first application has illustrated the implementation of the proposed methodology on a purely mathematical powerplant model, showcasing how the *powerplant management algorithm* satisfies power requirements based on user-defined parameters. In case ID 3-2, the algorithm's recommendation to switch to an alternative operational mode was justified by initially determining the minimum gas turbine throttle setting below which *mode 1* could no longer be sustained. Subsequently, an analytical relationship was derived to define the conditions required for *mode 1* to remain valid, as presented in Eq. (12).

The second case study has applied the developed powerplant model to a preliminarily sized regional propeller-driven aircraft, focusing on the cruise phase of a 300 nmi typical mission. By analyzing the total energy required to complete the mission profile as a function of varying fuel cell and battery throttle settings, the results have demonstrated how the powerplant model aids designers in identifying throttle combinations that minimize either overall energy consumption or CO_2 emissions. The model provides a straightforward and effective methodology for assessing each power source within a three-source powerplant architecture—an area where accessible evaluation methods are currently lacking. Furthermore, the throttle analysis conducted on the cruise phase can potentially be extended to other flight segments, enabling the identification of optimal throttle settings not only for individual mission phases but for the entire mission. Consequently, this establishes a robust framework for evaluating the performance of a three-source powertrain across a complete aircraft mission profile.

Owing to the assumed simplifications — such as the exclusion of transient effects and the omission of detailed component interactions — the proposed powerplant model proves particularly effective for analyzing powerplant applicability during the early stages of aircraft design. At a preliminary stage, exhaustive component data are often unavailable, and the development of complex simulation models is not feasible. Moreover, the model is inherently well-suited for energy optimization of hybrid-electric powerplants integrating up to three distinct energy sources, whether across an assigned mission profile or a specific flight trajectory. In conclusion, this model offers an effective methodology for minimizing the environmental impact of innovative aircraft platforms—a capability not provided by current state-of-the-art approaches. Existing methodologies (*e.g.*, *powertrain equations*) are limited in handling three-source powerplant architectures and rely on implicit parameters (*e.g.*, *supplied power ratios*) that do not allow direct control over the contribution of each power source.

CRediT authorship contribution statement

Giuseppe Grazioso: Writing – review & editing, Writing – original draft, Methodology, Conceptualization. **Mario Di Stasio:** Writing – review & editing, Writing – original draft, Conceptualization. **Fabrizio Nicolosi:** Writing – review & editing, Supervision, Funding acquisition, Conceptualization. **Salvatore Trepiccione:** Software, Methodology.

Declaration of competing interest

The authors declare the following financial interests/personal relationships which may be considered as potential competing interests: Fabrizio Nicolosi reports financial support was provided by HERA project. If there are other authors, they declare that they have no known competing financial interests or personal relationships that could have appeared to influence the work reported in this paper.

Acknowledgments

The research presented in this paper has been performed in the framework of the HERA project (Hybrid Electric Regional Aircraft) and has received funding from the European Union Clean Aviation Program under grant agreement n° 101102007.

Data availability

Data will be made available on request.

References

[1] European Parliament. Emissions from planes and ships: facts and figures (infographic). 2022, https://www.europarl.europa.eu/topics/en/article/20191129STO67756/emissions-from-planes-and-ships-facts-and-figures-infographic/. [Online; Accessed 05 November 2024].

[2] Chiara Massaro M, Pramotton S, Marocco P, Monteverde AHA, Santarelli M. Optimal design of a hydrogen-powered fuel cell system for aircraft applications. Energy Convers Manage 2024;306:118266. http://dx.doi.org/10.1016/j.enconman.2024.118266, URL https://www.sciencedirect.com/science/article/pii/S0196890424002073.

[3] European Commission and Research and Innovation general direction. Fly the green deal: Europe's vision for sustainable aviation. European Union publication office; 2022, http://dx.doi.org/10.2777/732726.

[4] Brelje BJ, Martins JR. Electric, hybrid, and turboelectric fixed-wing aircraft: A review of concepts, models, and design approaches. Prog Aerosp Sci 2019;104:1–19. http://dx.doi.org/10.1016/j.paerosci.2018.06.004, URL https://www.sciencedirect.com/science/article/pii/S0376042118300356.

[5] Abu Salem K, Palaia G, Quarta AA. Review of hybrid-electric aircraft technologies and designs: Critical analysis and novel solutions. Prog Aerosp Sci 2023;141:100924. http://dx.doi.org/10.1016/j.paerosci.2023.100924, URL https://www.sciencedirect.com/science/article/pii/S0376042123000404, Special Issue on Green Aviation.

[6] Thonemann N, Pierrat E, Dudka KM, Saavedra-Rubio K, Tromer Dragsdahl ALS, Laurent A. Towards sustainable regional aviation: Environmental potential of hybrid-electric aircraft and alternative fuels. Sustain Prod Consum 2024;45:371–85. http://dx.doi.org/10.1016/j.spc.2024.01.013, URL https://www.sciencedirect.com/science/article/pii/S2352550924000137.

[7] ATR. Turboprop market forecast 2022–2041. 2024, https://www.atr-aircraft.com/turboprop-market-forecast-2022-2041/. [Online; Accessed 06 November 2024].

[8] Bombardier. Bombardier aerospace releases annual business and commercial aircraft market forecasts. 2024, https://ir.bombardier.com/en/media/news/bombardier-aerospace-releases-annual-business-and-commercial-aircraft-market-forecasts. [Online; Accessed 06 November 2024].

[9] Pornet C, Isikveren A. Conceptual design of hybrid-electric transport aircraft. Prog Aerosp Sci 2015;79:114–35. http://dx.doi.org/10.1016/j.paerosci.2015.09.002, URL https://www.sciencedirect.com/science/article/pii/S0376042115300130.

[10] Voskuijl M, van Bogaert J, Rao AG. Analysis and design of hybrid electric regional turboprop aircraft. CEAS Aeronaut J 2018;9:15–25. http://dx.doi.org/10.1007/s13272-017-0272-1.

[11] Marciello V, Di Stasio M, Ruocco M, Trifari V, Nicolosi F, Meindl M, et al. Design exploration for sustainable regional hybrid-electric aircraft: A study based on technology forecasts. Aerospace 2023;10(2). http://dx.doi.org/10.3390/aerospace10020165, URL https://www.mdpi.com/2226-4310/10/2/165.

[12] Nasoulis CP, Protopapadakis GE, Ntouvelos EG, Gkoutzamanis VG, Kalfas A. Environmental and techno-economic evaluation for hybrid-electric propulsion architectures. Aeronaut J 2023;127:1904–26. http://dx.doi.org/10.1017/aer.2023.27.

[13] Viswanathan V, Epstein AH, Chiang Y-M, Takeuchi E, Bradley M, Langford J, et al. The challenges and opportunities of battery-powered flight. Nature 2022;601(7894):519–25. http://dx.doi.org/10.1038/s41586-021-04139-1.

[14] Khan FNU, Rasul MG, Sayem A, Mandal N. Maximizing energy density of lithium-ion batteries for electric vehicles: A critical review. Energy Rep 2023;9:11–21. http://dx.doi.org/10.1016/j.egyr.2023.08.069, URL https://www.sciencedirect.com/science/article/pii/S2352484723012118, Proceedings of 2022 7th International Conference on Renewable Energy and Conservation.

[15] Reid SJ, Perez RE, Jansen PW. Hybrid electric aircraft design with optimal power management. Aerosp Sci Technol 2024;154:109479. http://dx.doi.org/10.1016/j.ast.2024.109479, URL https://www.sciencedirect.com/science/article/pii/S1270963824006102.

[16] Hospodka J, Bínová H, Pleninger S. Assessment of all-electric general aviation aircraft. Energies 2020;13(23). http://dx.doi.org/10.3390/en13236206, URL https://www.mdpi.com/1996-1073/13/23/6206.

[17] Soleymani M, Mostafavi V, Hebert M, Kelouwani S, Boulon L. Hydrogen propulsion systems for aircraft, a review on recent advances and ongoing challenges. Int J Hydrog Energy 2024;91:137–71. http://dx.doi.org/10.1016/j.ijhydene.2024.10.131, URL https://www.sciencedirect.com/science/article/pii/S0360319924043295.

[18] Palladino V, Jordan A, Bartoli N, Schmollgruber P, Pommier-Budinger V, Benard E. Preliminary studies of a regional aircraft with hydrogen-based hybrid propulsion. In: AIAA Aviation 2021 forum. http://dx.doi.org/10.2514/6.2021-2411, arXiv:https://arc.aiaa.org/doi/pdf/10.2514/6.2021-2411, URL https://arc.aiaa.org/doi/abs/10.2514/6.2021-2411.

[19] Rischmüller UCJ, Lessis A, Egerer P, Hornung M. Conceptual design of a hydrogen-hybrid dual-fuel regional aircraft retrofit. Aerospace 2024;11(2). http://dx.doi.org/10.3390/aerospace11020123, URL https://www.mdpi.com/2226-4310/11/2/123.

[20] Ji Z, Rokni MM, Qin J, Zhang S, Dong P. Energy and configuration management strategy for battery/fuel cell/jet engine hybrid propulsion and power systems on aircraft. Energy Convers Manage 2020;225. http://dx.doi.org/10.1016/j.enconman.2020.113393.

[21] Eissele J, Lafer S, Mejía Burbano C, Schließus J, Wiedmann T, Mangold J, et al. Hydrogen-powered aviation—Design of a hybrid-electric regional aircraft for entry into service in 2040. Aerospace 2023;10(3). http://dx.doi.org/10.3390/aerospace10030277, URL https://www.mdpi.com/2226-4310/10/3/277.

[22] Sparano M, Sorrentino M, Troiano G, Cerino G, Piscopo G, Basaglia M, et al. The future technological potential of hydrogen fuel cell systems for aviation and preliminary co-design of a hybrid regional aircraft powertrain through a mathematical tool. Energy Convers Manage 2023;281:116822. http://dx.doi.org/10.1016/j.enconman.2023.116822, URL https://www.sciencedirect.com/science/article/pii/S0196890423001681.

[23] Zaghari B, Zhou T, Enalou HB, Pontika E, Laskaridis P. The impact of multi-stack fuel cell configurations on electrical architecture for a Zero Emission Regional aircraft. In: AIAA SCITECH 2023 forum. http://dx.doi.org/10.2514/6.2023-1593, arXiv:https://arc.aiaa.org/doi/pdf/10.2514/6.2023-1593, URL https://arc.aiaa.org/doi/abs/10.2514/6.2023-1593.

[24] Li Y, Hu Z, Zhang Y, Li J, Xu L, Ouyang M. Optimal performance and preliminary parameter matching for hydrogen fuel cell powertrain system of electric aircraft. ETransportation 2024;21:100342. http://dx.doi.org/10.1016/j.etran.2024.100342, URL https://www.sciencedirect.com/science/article/pii/S2590116824000328.

[25] Schenke F, Hoelzen J, Bredemeier D, Schomburg L, Bensmann A, Hanke-Rauschenbach R. LH2 supply for the initial development phase of H2-powered aviation. Energy Convers Management: X 2024;24:100797. http://dx.doi.org/10.1016/j.ecmx.2024.100797, URL https://www.sciencedirect.com/science/article/pii/S2590174524002757.

[26] Hoelzen J, Koenemann L, Kistner L, Schenke F, Bensmann A, Hanke-Rauschenbach R. H2-powered aviation – Design and economics of green LH2 supply for airports. Energy Convers Management: X 2023;20:100442. http://dx.doi.org/10.1016/j.ecmx.2023.100442, URL https://www.sciencedirect.com/science/article/pii/S2590174523000983.

[27] Hoelzen J, Flohr M, Silberhorn D, Mangold J, Bensmann A, Hanke-Rauschenbach R. H2-powered aviation at airports – Design and economics of LH2 refueling systems. Energy Convers Management: X 2022;14:100206. http://dx.doi.org/10.1016/j.ecmx.2022.100206, URL https://www.sciencedirect.com/science/article/pii/S2590174522000290.

[28] Alrebei OF, Alherbawi M, Thiehmed Z, Ismail R, Nasery M, Amhamed AI, et al. Aircraft performance of a novel SAF: Lower costs, lower environmental impact, and higher aircraft performance. Energy Convers Management: X 2024;24. http://dx.doi.org/10.1016/j.ecmx.2024.100739.

[29] Nam T, Soban D, Mavris D. A generalized aircraft sizing method and application to electric aircraft. In: 3rd international energy conversion engineering conference. 2012, http://dx.doi.org/10.2514/6.2005-5574, arXiv:https://arc.aiaa.org/doi/pdf/10.2514/6.2005-5574, URL https://arc.aiaa.org/doi/abs/10.2514/6.2005-5574.

[30] Buecherl D, Bolvashenkov I, Herzog H-G. Verification of the optimum hybridization factor as design parameter of hybrid electric vehicles. In: IEEE vehicle power and propulsion conference. 2009, p. 847–51. http://dx.doi.org/10.1109/VPPC.2009.5289758.

[31] Pornet C, Gologan C, Vratny PC, Seitz A, Schmitz O, Isikveren AT, et al. Methodology for sizing and performance assessment of hybrid energy aircraft. J Aircr 2015;52(1):341–52. http://dx.doi.org/10.2514/1.C032716.

[32] Isikveren A, Kaiser S, Pornet C, Vratny P. Pre-design strategies and sizing techniques for dual-energy aircraft. Aircr Eng Aerosp Technol 2014;86:525–42. http://dx.doi.org/10.1108/AEAT-08-2014-0122.

[33] de Vries R, Brown M, Vos R. Preliminary sizing method for hybrid-electric distributed-propulsion aircraft. J Aircr 2019;56(6):2172–88. http://dx.doi.org/10.2514/1.C035388.

[34] Palaia G, Abu Salem K. Mission performance analysis of hybrid-electric regional aircraft. Aerospace 2023;10(3). http://dx.doi.org/10.3390/aerospace10030246, URL https://www.mdpi.com/2226-4310/10/3/246.

[35] Schröder M, Becker F, Kallo J, Gentner C. Optimal operating conditions of PEM fuel cells in commercial aircraft. Int J Hydrog Energy 2021;46:33218–40. http://dx.doi.org/10.1016/j.ijhydene.2021.07.099.

[36] Schröder M, Becker F, Gentner C. Optimal design of proton exchange membrane fuel cell systems for regional aircraft. Energy Convers Manage 2024;308. http://dx.doi.org/10.1016/j.enconman.2024.118338.

[37] Abdelhedi F, Jarraya I, Bawayan H, Abdelkeder M, Rizoug N, Koubaa A. Optimizing electric vehicles efficiency with hybrid energy storage: Comparative analysis of rule-based and neural network power management systems. Energy 2024;133979. http://dx.doi.org/10.1016/j.energy.2024.133979, URL https://www.sciencedirect.com/science/article/pii/S0360544224037575.

[38] Zhang J, Roumeliotis I, Zolotas A. Nonlinear model predictive control-based optimal energy management for hybrid electric aircraft considering aerodynamics-propulsion coupling effects. IEEE Trans Transp Electrification 2022;8(2):2640–53. http://dx.doi.org/10.1109/TTE.2021.3137260.

[39] Misley A, D'Arpino M, Ramesh P, Canova M. A real-time energy management strategy for hybrid electric aircraft propulsion systems. In: 2021 AIAA/IEEE electric aircraft technologies symposium. 2021, p. 1–11. http://dx.doi.org/10.23919/EATS52162.2021.9704831.

[40] Tan H, Zhang H, Peng J, Jiang Z, Wu Y. Energy management of hybrid electric bus based on deep reinforcement learning in continuous state and action space. Energy Convers Manage 2019;195:548–60. http://dx.doi.org/10.1016/j.enconman.2019.05.038, URL https://www.sciencedirect.com/science/article/pii/S019689041930593X.

[41] Cao Y, Yao M, Sun X. An overview of modelling and energy management strategies for hybrid electric vehicles. Appl Sci 2023;13(10). http://dx.doi.org/10.3390/app13105947, URL https://www.mdpi.com/2076-3417/13/10/5947.

[42] Xie Y, Savvarisal A, Tsourdos A, Zhang D, Gu J. Review of hybrid electric powered aircraft, its conceptual design and energy management methodologies. Chin J Aeronaut 2021;34(4):432–50. http://dx.doi.org/10.1016/j.cja.2020.07.017, URL https://www.sciencedirect.com/science/article/pii/S1000936120303368.

[43] Pinto Leite JPS, Voskuijl M. Optimal energy management for hybrid-electric aircraft. Aircr Eng Aerosp Technol 2020;92(6):851–61. http://dx.doi.org/10.1108/AEAT-03-2019-0046.

[44] Doff-Sotta M, Cannon M, Bacic M. Optimal energy management for hybrid electric aircraft. IFAC- Pap 2020;53:6043–9.

[45] Doff-Sotta M, Cannon M, Bacic M. Predictive energy management for hybrid electric aircraft propulsion systems. IEEE Trans Control Syst Technol 2022;PP:1. http://dx.doi.org/10.1109/TCST.2022.3193295.

[46] Li S, Gu C, Zhao P, Cheng S. A novel hybrid propulsion system configuration and power distribution strategy for light electric aircraft. Energy Convers Manage 2021;238:114171. http://dx.doi.org/10.1016/j.enconman.2021.114171, URL https://www.sciencedirect.com/science/article/pii/S0196890421003472.

[47] Gudmundsson S. General aviation aircraft design: applied methods and procedures. Elsevier Inc; 2014, http://dx.doi.org/10.1016/C2011-0-06824-2.

[48] Brent RP. Algorithm for minimization without derivatives. Prentice-Hall; 1973.

[49] Hybrid Electric Regional Architecture (HERA) Project. 2025, https://project-hera.eu/home. [Online; Accessed 18 February 2025].